Bipod flexure for 1-m primary mirror system

Article *in* The Review of scientific instruments · December 2014

DOI: 10.1063/1.4902151 · Source: PubMed

3 authors, including:

Hag-Yong Kihm
Korea Research Institute of Standards and Science
43 PUBLICATIONS **344** CITATIONS

SEE PROFILE

Yun-Woo Lee
Korea Research Institute of Standards and Science
169 PUBLICATIONS **1,261** CITATIONS

SEE PROFILE

AIP | Review of Scientific Instruments

Bipod flexure for 1-m primary mirror system

Hagyong Kihm, Ho-Soon Yang, and Yun-Woo Lee

Citation: Review of Scientific Instruments **85**, 125101 (2014); doi: 10.1063/1.4902151
View online: http://dx.doi.org/10.1063/1.4902151
View Table of Contents: http://scitation.aip.org/content/aip/journal/rsi/85/12?ver=pdfcov
Published by the AIP Publishing

Bipod flexure for 1-m primary mirror system

Hagyong Kihm,[a] Ho-Soon Yang, and Yun-Woo Lee
Center for Space Optics, Korea Research Institute of Standards and Science, Daejeon 305-340, South Korea

(Received 17 August 2014; accepted 7 November 2014; published online 1 December 2014)

We present an analytical formulation of the bipod flexure for mounting the 1-m primary mirror in a space telescope. Compliance and stiffness matrices of the bipod flexure are derived to estimate theoretical performance and to make initial design guidelines. We use finite element analysis to optimize the bipod design satisfying the application requirements. Experimental verification is achieved by vibration test with a dummy mirror system. © *2014 AIP Publishing LLC*. [http://dx.doi.org/10.1063/1.4902151]

I. INTRODUCTION

Optical elements such as telescope mirrors usually require mounting supports to maintain their optical performance under environmental disturbances. In case of satellite telescopes, the mirror mount should secure the optics' safety against launch loads and thermal variations while operating in earth's orbit. A kinematic mount is an ideal support for optical elements, but the point contact is not feasible in environmentally challenged systems. Instead, a semi-kinematic mount with a finite contact area is usually adopted to dissipate local stresses. Flexure mounting can be regarded as a semi-kinematic support. A flexure is a monolithic structure providing elastic motions in a predefined way. The benefits of using flexures include lack of hysteresis and the friction effects inherent in semi-kinematic mounts. Also, maintenance is unnecessary and fabrication has become common practice with electrical discharge machining.

A mirror mount flexure is not intended for linear or precise motions. Different from the flexure hinges used in actuator mechanism, a mirror mount flexure minimizes optical surface distortions and maintains optical alignment under operation or transport. The location and direction of a mounting flexure is determined by the kinematic principles. The line of action of the flexure should pass through the mirror's gravity center. Compliance should be provided to athermalize the mirror and mounting flexures. For example, radial compliance should be added in axisymmetric mirror element. Tangential compliance is also required to prevent assembly stress from propagating toward the mirror surface.[1] Lateral mirror supports are usually responsible for radial and tangential compliance. Axial mirror supports in case of massive large aperture telescopes reduce mirror surface deformation.

Flexure mounts can be categorized according to the type of flexure element. Simple blade flexures are usually adopted for relatively small axisymmetric mirrors as tangential edge supports.[1] Flexure hinges can also be categorized according to the shape of cross section. There are cornet-filleted flexure hinges and conic-section flexure hinges such as circular, elliptical, parabolic, and hyperbolic.[2–4] Corner-filleted flexures are more bending-compliant and induce lower stresses. Less precision in rotational motion is not a matter of concern in mirror mount flexures. Most mirror mount flexures, be it blade or bipod, has corner-filleted cross sections for those reasons.[5]

Bipod flexure, which is the most common support type, is a combination of two blade flexures forming a triangle and generally gives better results in terms of optical performances.[6,7] We reported an adjustable bipod flexure for mounting the 800-mm primary mirror in a space telescope.[8] We used FEA (finite element analysis) as an initial design and optimization tool for the flexure, and verified the design with experimental results obtained from vibration tests and optical interferometric testing. Initial design of the bipod flexures required exhaustive iterations with modeling and FEA tools to explore multidimensional space. Also the intrinsic characteristics of the compliance of the bipod were not explicitly identified. Therefore, the performance sensitivity to dimensional parameters, which is necessary for tolerance analysis, required extensive FEA with small dimensional disturbances. Without resorting to theoretical formulations, the design task was time-consuming and needed a lot of trials and errors.

On the other hand, optimal design of flexure hinges is possible for precision mechanisms based on theoretical closed form solutions[9,10] or finite element analysis.[11] Empirical formulation and dimensionless graph analysis was also reported.[3,12] Those researches are valuable providing initial design steps and even optimizing simple cases when it comes to stages and precision mechanisms. Mirror mount flexures can also benefit from those results as design guidelines.

In this paper, we propose an analytical formulation of the bipod flexure for an optical mirror mount. We derive the compliance and stiffness matrices of the bipod flexure following the approach based on the screw theory proposed by Su.[13] Theoretical performance estimation is possible simply by replacing the flexure's dimensional parameters with numerical values. For example, the relation between fundamental frequency of the mirror system and each flexure dimension can be investigated using a stiffness matrix. Displacement of the mirror's surface can also be estimated using a compliance matrix. We use the theoretical formulation for the initial flexure design of 1-m mirror system. Experimental verification is achieved by vibration tests with a dummy mirror system. Section II describes the analytical formulation of the bipod flexure and derives compliance and stiffness matrices. Section III explains a dummy mirror system for the space qualification of bipod flexures. Design details and FEA results are shown.

[a]Author to whom correspondence should be addressed. Electronic mail: hkihm@kriss.re.kr

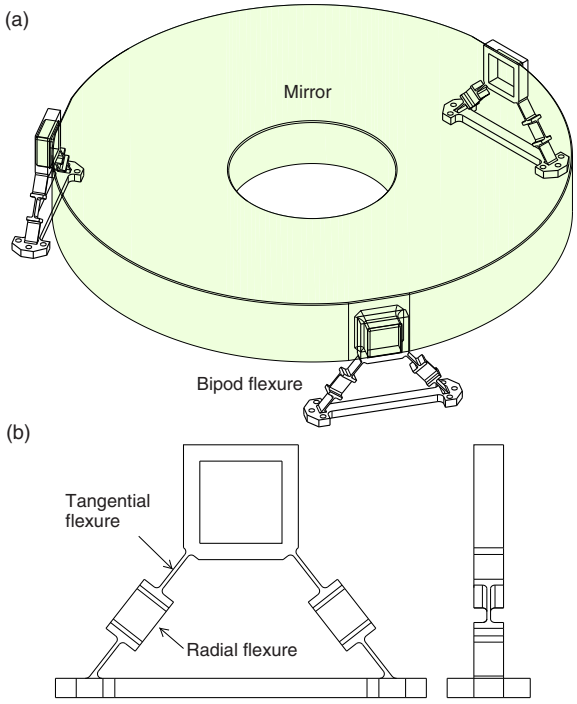

FIG. 1. (a) Conventional bipod flexures are assembled with a primary mirror. (b) The monolithic bipod flexure is composed of two tangential flexures and a radial flexure for the symmetric half.

Section IV shows the results of vibration tests and verifies its application in a space optical system. Section V concludes this paper.

II. COMPLIANCE AND STIFFNESS OF BIPOD FLEXURE

The conventional bipod flexures supporting a primary mirror is shown in Fig. 1(a). The mirror has three square bosses made at the mirror's rim for flexure mounting. The monolithic flexure is coupled with the mirror by using an epoxy adhesive. The apex of the triangle formed by a bipod flexure should point to the mass center of the mirror or equivalently the shear center of the mirror such that gravity-induced surface distortion can be effectively reduced.[8] Each bipod flexure has a symmetric combination of two tangential blades and a radial blade as shown in Fig. 1(b), and they are named after the role of each part. Tangential flexures give tangential compliance when the mirror is accelerated in lateral directions or perpendicular to the mirror's optic axis. Radial flexure affords radial compliance to the mirror, whereby radial expansion of the mirror due to thermal loads can be compensated, for example.

In order to formulate the complicated stiffness matrix of the bipod flexure, the structure is divided into each element. The connectivity of individual elements or building blocks is systematically characterized by coordinate transformation of screws (twists and wrenches).[13] The following is the procedure to derive a symbolic formulation of a bipod flexure and its combination as a mirror mount.

(1) Compliance matrices for each tangential and radial blade flexures are derived, which are explained in Secs. II A and II B.

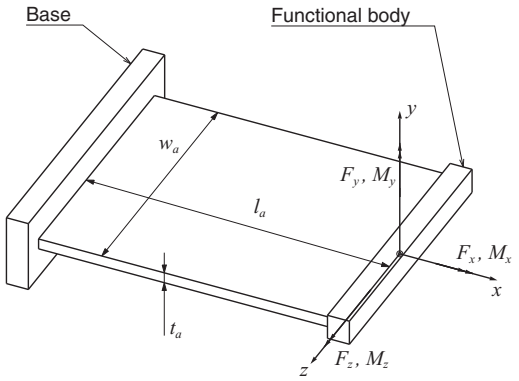

FIG. 2. A tangential blade flexure with a rectangular cross section. The thickness is much smaller than the length, i.e., $t_a \ll l_a$.

(2) Using a serial compliance summation, two tangential blades and a radial blade are combined to form a symmetric half of the bipod, which is explained in Sec. II C.
(3) Using a parallel stiffness summation, a bipod flexure is formulated based on the results of the previous step.
(4) We, then, combine stiffness matrices of three bipod flexures after respective coordinate transformation according to the mount configuration, which is explained in Sec. II E. The subsequent sections explain the above steps using the nomenclature in Su's paper.[13]

A. Tangential blade flexure

Figure 2 shows a tangential blade flexure with a rectangular cross section of length l_a, thickness t_a, and width w_a. The coordinate frame is located at the functional body, as we are interested in the motion at the end. Let us denote the deformation by a general twist $\hat{T} = (\theta_x, \theta_y, \theta_z; \delta_x, \delta_y, \delta_z)$ and the loading by a wrench $\hat{W} = (F_x, F_y, F_z; M_x, M_y, M_z)$. Both are column vectors. The goal is to derive the mapping from $\hat{W}$ to $\hat{T}$ in terms of geometric and material parameters of the flexure. Applying the principle of linear elastic theory for sufficiently small deformations, the deformation twist and the loading wrench are related by

$$\hat{T} = [C]\,\hat{W}, \quad \hat{W} = [K]\,\hat{T}, \quad [C] = [K]^{-1}, \qquad (1)$$

where $[C]$ and $[K]$ are 6×6 compliance and stiffness matrices, respectively.

The compliance matrix for the blade flexure, which is already derived in Eq. (9) of Ref. 13, is repeated in Eq. (2),

$$[C_a] = \begin{bmatrix} 0 & 0 & 0 & \frac{l_a}{GJ} & 0 & 0 \\ 0 & 0 & \frac{-6l_a^{\,2}}{t_a w_a^{\,3} E} & 0 & \frac{12 l_a}{t_a w_a^{\,3} E} & 0 \\ 0 & \frac{6l_a^{\,2}}{t_a^{\,3} w_a E} & 0 & 0 & 0 & \frac{12 l_a}{t_a^{\,3} w_a E} \\ \frac{la}{t_a w_a E} & 0 & 0 & 0 & 0 & 0 \\ 0 & \frac{4l_a^{\,3}}{t_a^{\,3} w_a E} & 0 & 0 & 0 & \frac{6l_a^{\,2}}{t_a^{\,3} w_a E} \\ 0 & 0 & \frac{4l_a^{\,3}}{t_a w_a^{\,3} E} & 0 & \frac{-6l_a^{\,2}}{t_a^{\,3} w_a^{\,3} E} & 0 \end{bmatrix}, \qquad (2)$$

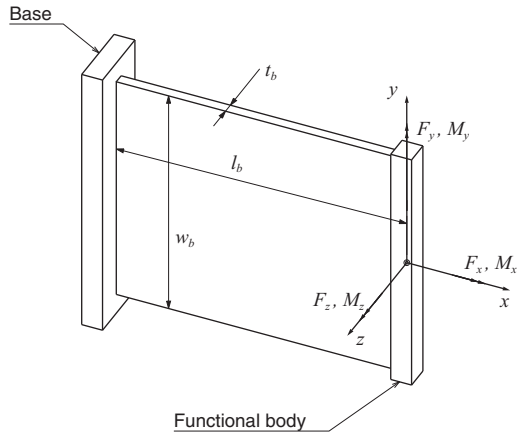

FIG. 3. A radial blade flexure with a rectangular cross section. The thickness is much smaller than the length, i.e., $t_b \ll l_b$.

where E and G are the Young's and shear modulus, and J is the torsion constant. It can be seen that $[C_a]$ is determined by five independent design parameters $P = (E, G, t_a, w_a, l_a)$.

B. Radial blade flexure

Radial flexure in Fig. 1(b) connects two tangential flexures, and the compliance of the radial flexure element can be derived with coordinate frame shown in Fig. 3. The compliance of the radial blade flexure can be derived easily just by exchanging the parameter t and w in Eq. (2), and it is written in Eq. (3),

$$[C_b] = \begin{bmatrix} 0 & 0 & 0 & \frac{l_b}{GJ} & 0 & 0 \\ 0 & 0 & \frac{-6{l_b}^2}{{w_b}{t_b}^3 E} & 0 & \frac{12 l_b}{{w_b}{t_b}^3 E} & 0 \\ 0 & \frac{6{l_b}^2}{{w_b}^3 t_b E} & 0 & 0 & 0 & \frac{12 l_b}{{w_b}^3 t_b E} \\ \frac{l_b}{w_b t_b E} & 0 & 0 & 0 & 0 & 0 \\ 0 & \frac{4{l_b}^3}{{w_b}^3 t_b E} & 0 & 0 & 0 & \frac{6 l_b^2}{{w_b}^3 t_b E} \\ 0 & 0 & \frac{4{l_b}^3}{{w_b}{t_b}^3 E} & 0 & \frac{-6{l_b}^2}{{w_b}{t_b}^3 E} & 0 \end{bmatrix}. \quad (3)$$

C. Combination of tangential and radial flexures

A symmetric half of the bipod flexure in Fig. 4 is formed by a serial chain of two tangential flexures and a radial flexure. The deformation of the functional body is the superimposition of the deformation of individual elements. Therefore, the overall compliance of the serial flexure chain in Fig. 4 is the summation of each compliance matrix in the same coordinate frame. Coordinate transformation is necessary for the compliance matrices in Eqs. (2) and (3), and the overall compliance matrix is calculated as

$$[C_t] = [Ad_a][C_a][Ad_a]^{-1} + [Ad_b][C_b][Ad_b]^{-1} + [C_c], \quad (4)$$

where $[Ad_{a,b}]$ is the coordinate transformation matrix for the flexure a, b to the functional body. $[Ad_{a,b}]$ is a 6×6 adjoint

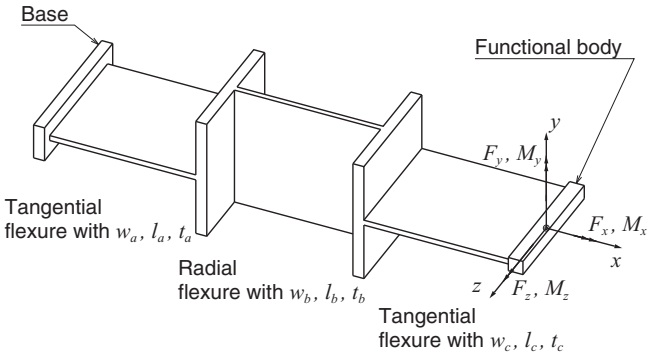

FIG. 4. A combination of two tangential flexures and a radial flexure forms the symmetric half of a bipod flexure.

transformation matrix, and can be written as

$$[Ad] = \begin{bmatrix} R & 0 \\ DR & R \end{bmatrix}, \quad (5)$$

where R is the 3×3 rotation matrix and D is the skew symmetric matrix defined by the translational vector as shown in Eq. (6),

$$[R_a] = [R_b] = [I],$$
$$[D_a] = \begin{bmatrix} 0 & 0 & 0 \\ 0 & 0 & l_b + l_c \\ 0 & -l_b - l_c & 0 \end{bmatrix}, \quad [D_b] = \begin{bmatrix} 0 & 0 & 0 \\ 0 & 0 & l_c \\ 0 & -l_c & 0 \end{bmatrix}. \quad (6)$$

For simplicity, if we assume $t_a = t_b = t_c = t$, $w_a = w_b = w_c = w$, and $l_a = l_b = l_c = l$, the compliance matrix of the flexure in Fig. 4 is calculated as

$$[C_t] = \begin{bmatrix} 0 & 0 & 0 & \frac{3l}{GJ} & 0 & 0 \\ 0 & 0 & \frac{-18l^2(2t^2+w^2)}{t^3 w^3 E} & 0 & \frac{12l(2t^2+w^2)}{t^3 w^3 E} & 0 \\ 0 & \frac{18l^2(t^2+2w^2)}{t^3 w^3 E} & 0 & 0 & 0 & \frac{12l(t^2+2w^2)}{t^3 w^3 E} \\ \frac{3l}{twE} & 0 & 0 & 0 & 0 & 0 \\ 0 & \frac{4l^3(7t^2+20w^2)}{t^3 w^3 E} & 0 & 0 & 0 & \frac{18l^2(t^2+2w^2)}{t^3 w^3 E} \\ 0 & 0 & \frac{4l^3(20t^2+7w^2)}{t^3 w^3 E} & 0 & \frac{-18l^2(2t^2+w^2)}{t^3 w^3 E} & 0 \end{bmatrix}. \quad (7)$$

We also assume that the thickness of two connecting bodies between blade flexures is much smaller than the flexure length and can be neglected.

D. Bipod flexure

A bipod flexure is formed by connecting a functional body to a reference body through two combinations of tangential and radial flexures as shown in Fig. 5. Let us denote the stiffness matrix of the jth flexure element by $[K_j]$. For the same displacement of the functional body, the force required will be the sum of forces required for each element. As in serial flexure chains, all loads must be written in the same coordinate frame. Mathematically the overall stiffness matrix of

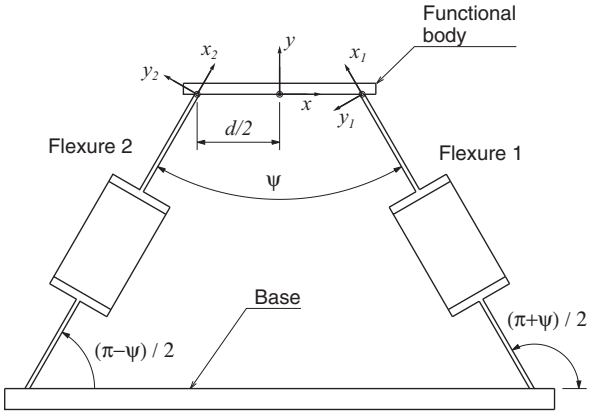

FIG. 5. A bipod flexure is formed by two parallel flexures made of radial and tangential blade flexures.

a parallel flexure chain is calculated as

$$[K_p] = \sum_{j=0}^{m} [Ad_j][K_j][Ad_j]^{-1}, \tag{8}$$

where $[Ad_j]$ is the coordinate transformation operator from the jth flexure to the functional body.

The bipod flexure in Fig. 5 has a trapezoidal pivot that is formed by two identical blade flexures assembled symmetrically by an angle of ψ at a distance d. The coordinate transformations for flexure 1 and 2 are, respectively,

$$[R_1] = \left[Z\left(\tfrac{\pi+\psi}{2}\right)\right] = \begin{bmatrix} \cos\left(\frac{\pi+\psi}{2}\right) & -\sin\left(\frac{\pi+\psi}{2}\right) & 0 \\ \sin\left(\frac{\pi+\psi}{2}\right) & \cos\left(\frac{\pi+\psi}{2}\right) & 0 \\ 0 & 0 & 1 \end{bmatrix},$$

$$[R_2] = \left[Z\left(\tfrac{\pi-\psi}{2}\right)\right] = \begin{bmatrix} \cos\left(\frac{\pi-\psi}{2}\right) & -\sin\left(\frac{\pi-\psi}{2}\right) & 0 \\ \sin\left(\frac{\pi-\psi}{2}\right) & \cos\left(\frac{\pi-\psi}{2}\right) & 0 \\ 0 & 0 & 1 \end{bmatrix},$$

$$[D_1] = \begin{bmatrix} 0 & 0 & 0 \\ 0 & 0 & -d/2 \\ 0 & d/2 & 0 \end{bmatrix}, \quad [D_2] = \begin{bmatrix} 0 & 0 & 0 \\ 0 & 0 & d/2 \\ 0 & -d/2 & 0 \end{bmatrix}. \tag{9}$$

Substituting the above transformation matrices and $[K_t]$, which is the inverse of $[C_t]$ shown in Eq. (7), into Eq. (8) to obtain the following stiffness matrix:

$$[K_p] = [Ad_1][K_t][Ad_1]^{-1} + [Ad_2][K_t][Ad_2]^{-1}. \tag{10}$$

And the compliance matrix is computed as

$$[C_p] = [K_p]^{-1} = \begin{bmatrix} 0 & 0 & C^p_{13} & C^p_{14} & 0 & 0 \\ 0 & 0 & 0 & 0 & C^p_{25} & 0 \\ C^p_{31} & 0 & 0 & 0 & 0 & C^p_{36} \\ C^p_{41} & 0 & 0 & 0 & 0 & C^p_{46} \\ 0 & C^p_{52} & 0 & 0 & 0 & 0 \\ 0 & 0 & C^p_{63} & C^p_{64} & 0 & 0 \end{bmatrix}, \tag{11}$$

where C^p_{ij} are the nonzero compliance elements and they are expressed in the Appendix. Let us take a look at the compliance of this flexure pivot subject to a moment loading M_z. The element C^p_{36} represents the deformation θ_z due to the loading M_z, and C^p_{46} is the parasitic translational deformation δ_x. To determine the position of the instant rotation center on the y axis, we compute

$$\frac{C^p_{46}}{C^p_{36}} = -\frac{\cos\frac{\psi}{2}\left\{9l + d(3-\alpha^2-26\beta^2)\sin\frac{\psi}{2}\right\}}{3+\alpha^2+26\beta^2+(3-\alpha^2-26\beta^2)\cos}, \tag{12}$$

where $\alpha = l/w$ and $\beta = l/t$. It is intuitive to see that the nominal instant center is at the point $(0, (d/2)\cot(\psi/2), 0)$ on the y axis, which is the intersection point of two flexures in Fig. 5. The parasitic error of the instant center is calculated as

$$\Delta_{ry} = \frac{C^p_{46}}{C^p_{36}} - \frac{d\cot\frac{\psi}{2}}{2}$$

$$= -\frac{3\cot\frac{\psi}{2}\left(d + 3l\sin\frac{\psi}{2}\right)}{3+\alpha^2+26\beta^2+(3-\alpha^2-26\beta^2)\cos\psi}, \tag{13}$$

The error Δ_{ry} becomes larger as the bipod angle ψ gets smaller. This formula helps to decide the appropriate angle ψ and the position of mirror boss with respect to the gravity center of a mirror system.

E. Combination of three bipod flexures

The primary mirror system is formed by three identical flexures assembled symmetrically in parallel. To investigate the overall compliance/stiffness of the mirror system, we need to derive the transformation matrix from the local coordinate system at each bipod flexure to the functional body space (coordinate frame on the mirror). For bipod flexure 1, the coordinate transformation is obtained by the geometry shown in Fig. 6, written as

$$[R_1] = [I], [D_1] = \begin{bmatrix} 0 & 0 & 0 \\ 0 & 0 & -d/2 \\ 0 & d/2 & 0 \end{bmatrix}. \tag{14}$$

And the transformation for bipod 2 and 3, $[R_2]$, $[D_2]$, $[R_3]$, $[D_3]$ are obtained by rotating the coordinate x, y, z about y axis for $2\pi/3$ and $-2\pi/3$, respectively. More specifically, they are written as

$$[R_2] = \left[Y\left(\tfrac{2\pi}{3}\right)\right] = \begin{bmatrix} -\frac{1}{2} & 0 & \frac{\sqrt{3}}{2} \\ 0 & 1 & 0 \\ -\frac{\sqrt{3}}{2} & 0 & -\frac{1}{2} \end{bmatrix},$$

$$[R_3] = \left[Y\left(-\tfrac{2\pi}{3}\right)\right] = \begin{bmatrix} -\frac{1}{2} & 0 & -\frac{\sqrt{3}}{2} \\ 0 & 1 & 0 \\ \frac{\sqrt{3}}{2} & 0 & -\frac{1}{2} \end{bmatrix},$$

$$[D_2] = \begin{bmatrix} 0 & \frac{r}{2} & 0 \\ -\frac{r}{2} & 0 & -\frac{\sqrt{3}}{2}r \\ 0 & \frac{\sqrt{3}}{2}r & 0 \end{bmatrix}, \quad [D_3] = \begin{bmatrix} 0 & \frac{r}{2} & 0 \\ -\frac{r}{2} & 0 & \frac{\sqrt{3}}{2}r \\ 0 & -\frac{\sqrt{3}}{2}r & 0 \end{bmatrix}. \tag{15}$$

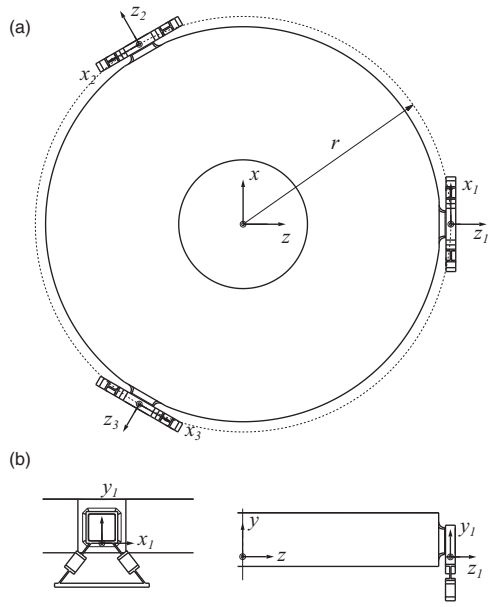

FIG. 6. A primary mirror mounted with three identical bipod flexures is shown with their coordinates. (a) is the upper view and (b) is the side view of the system.

The stiffness matrix $[K]$ can be obtained with the following equation:

$$[K] = \sum_{j=1}^{3} [Ad_j][K_j][Ad_j]^{-1}. \tag{16}$$

We, then, compute the compliance matrix of the mirror system by inverting the stiffness matrix $[K]$ as shown in Eq. (17). Each element can be derived easily with the help of modern algebraic software, such as Mathematica® or Maple®,

$$[C] = [K]^{-1} = \begin{bmatrix} 0 & 0 & c_{13} & c_{14} & 0 & 0 \\ 0 & 0 & 0 & 0 & c_{25} & 0 \\ c_{31} & 0 & 0 & 0 & 0 & c_{36} \\ c_{41} & 0 & 0 & 0 & 0 & c_{46} \\ 0 & c_{52} & 0 & 0 & 0 & 0 \\ 0 & 0 & c_{63} & c_{64} & 0 & 0 \end{bmatrix}. \tag{17}$$

The instant rotation center for forces F_x and F_z can be obtained by computing

$$\frac{c_{41}}{c_{31}} = -\frac{c_{63}}{c_{13}} = c_y. \tag{18}$$

This shows that when a lateral force F_x is applied, the motion of the mirror is instantaneously equivalent to a rotation about the line through the instant rotation center parallel to z axis. Similarly, a force F_z will cause a rotation about the line through the center and parallel to x axis. The instant rotation center in Eq. (18) is located far away from the mirror system, whereas the rotation center of the bipod flexure itself in Eq. (12) is near the mass center of the system. The translational compliance along x and z axes is the same due to the symmetry, calculated as

$$\frac{\delta_x}{F_x} = \frac{\delta_z}{F_z} = c_{41} = c_{63}. \tag{19}$$

From this result, we can expect the translational stiffnesses along x and z axes are the same, and there will be the same modal frequencies in each direction. This is verified from the FEA results and vibration experiments presented in Secs. III–IV.

III. BIPOD FLEXURE DESIGN AND ANALYSIS

As initial design guidelines for the bipod flexure, we can use the compliance/stiffness matrix derived in Sec. II. Parametric exploration of the initial design space satisfying the design requirements can be achieved easily without resorting to FEA. With stiffness $[K]$ in Eq. (16), we can calculate the fundamental frequency and find appropriate combinations of flexure dimensions. With compliance $[C]$ in Eq. (17), displacement of the mirror system under 1 g gravity can be found. Therefore, we can keep the allowable displacement required for aligning and testing the optical components. Also the bipod angle ψ minimizing the surface deformation of the mirror can be approximated with Eq. (12) and is used as an initial guess for further optimization using FEA.

With the specification for the 1-m primary mirror,[14,15] we explored the flexure design space. The mirror is made of Zerodur® and its weight is 46 kg. When the mirror system is in the horizontal setup for testing or assembly on the ground, the mirror's decenter due to gravity should be less than 20 μm. Also the fundamental frequency should be higher than 120 Hz. We can obtain the mirror's decenter using Eq. (19). For example, δ_x, the mirror's decenter in x direction is calculated as $C_{41} \cdot F_x = C_{41} \cdot m \cdot g = C_{41} \cdot (46\ kg) \cdot (9.81\ m/s^2)$ by assuming $M_z = 0$, as there is no moment applied in z direction. Also the weight of the bipod flexures is neglected. Figure 7 shows the plots of $\delta_x (= \delta_z)$ for the variation of each parameter when the others are fixed at nominal values. Each flexure dimension t, l, w, and ψ is normalized in the plot, and the ranges of actual values are noted in the figure. The design space satisfying the requirement can be used as a design guideline. The requirement for mirror's decenter is indicated with an arrow and most parametric ranges satisfy the requirement except for the flexure thickness t in the lower values. Also, t is the most sensitive dimensional parameter, and its tolerance should be carefully determined.

On the other hand, the fundamental frequency F_1 of the mirror system can be obtained by using Eq. (17). The only force applied to the system is its inertia due to gravity or acceleration from the support. In the vibration test, the mirror system is accelerated in each direction and the first natural frequency or the fundamental frequency occurs in the direction of maximum compliance. By comparing compliance elements of the first three columns in Eq. (17), we can expect the fundamental frequency and its modal participation. In our mirror system, the modal behaviour of the fundamental frequency is the lateral translation which is in x or z direction. This is also proven in the 800-mm mirror system.[8] In such cases, the fundamental frequency F_1 can be calculated using

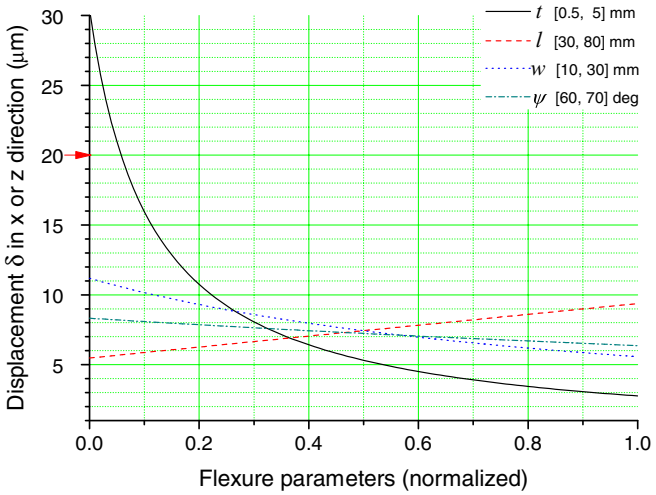

FIG. 7. Displacement δ of the mirror system under 1 g gravity in x or z direction. δ is obtained by using Eq. (19) when the dimensional parameter is changed in the ranges shown in the legend. The horizontal axis is normalized in each parameter for comparison. The design requirement is indicated with an arrow on the vertical axis. The parameters have nominal values of $t = 2$ mm, $l = 40$ mm, $w = 30$ mm, $\psi = 64°$.

C_{41} or C_{63} in Eq. (19), and can be expressed as

$$F_1 = \frac{1}{2\pi\sqrt{mC_{41}}} = \frac{1}{2\pi\sqrt{mC_{63}}}. \quad (20)$$

Figure 8 shows the plots F_1 for the variation of each parameter when the others are fixed at nominal values. Each flexure dimension t, l, w, and ψ is normalized in the plot, and the ranges of actual values are noted in the figure. Most parametric ranges satisfy the requirement of minimum 120 Hz, but the flexure thickness t should be thick enough to get margins for the requirement. We can use Figs. 7 and 8

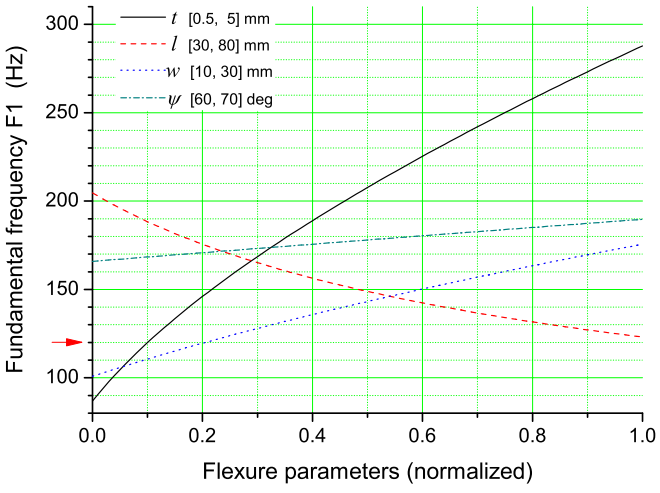

FIG. 8. Fundamental frequency F1 of the mirror system with respect to the variation of flexure parameters. F1 is obtained by using Eq. (20) when the dimensional parameter is changed in the ranges shown in the legend. The horizontal axis is normalized in each parameter for comparison. The design requirement is indicated with an arrow on the vertical axis. The parameters have nominal values of $t = 2$ mm, $l = 40$ mm, $w = 30$ mm, $\psi = 64°$.

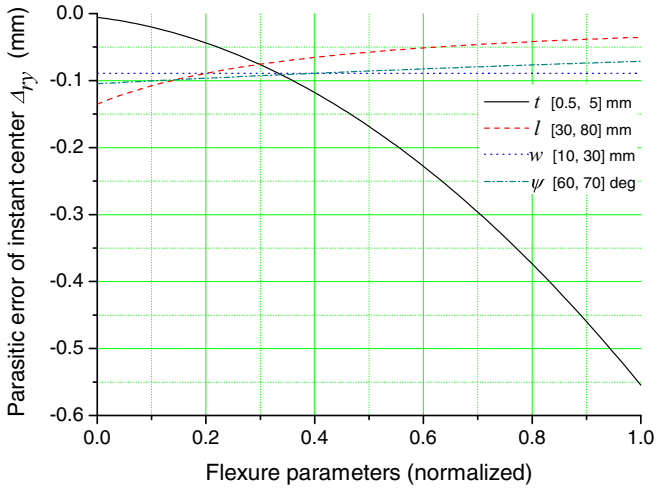

FIG. 9. Parasitic error of the instant rotation center Δ_{ry} with respect to the bipod flexure parameters. Δ_{ry} is obtained by using Eq. (13) when the dimensional parameter is changed in the ranges shown in the legend. The horizontal axis is normalized in each parameter for comparison. The parameters have nominal values of $t = 2$ mm, $l = 40$ mm, $w = 30$ mm, $\psi = 64°$.

or their equations when exploring the dimensional space with design of experiments or optimization routines.

Mirror's surface distortion due to 1 g gravity on the ground hinders testing and aligning the whole optical system. But bipod flexure is known to minimize the gravity induced distortions and we proposed the adjustable bipod flexure using shims (ABS) for mounting the mirror, of which performance was already verified with an 800-mm mirror system.[8] The angle of the bipod ψ has a relatively weak sensitivity to the mechanical performances as shown in Figs. 7 and 8. But the optical performance is greatly affected by the angle ψ, and determining the initial angle for further optimization is important. The instant rotation center of the flexure should be in the plane of mirror system's mass center. The parasitic error Δ_{ry} of the instant rotation center, which is Eq. (13), informs the position of the flexure with respect to the mirror. Figure 9 shows the plots Δ_{ry} for the variation of each parameter when the others are fixed at nominal values. The flexure thickness t is shown to be the most dominant parameter affecting Δ_{ry}, where the error increases nonlinearly as t becomes thicker. Δ_{ry} is almost -0.1 mm for the other parametric variations when t is at the nominal value of 2 mm. In that case, the mirror's mass center should be placed 0.1 mm below the nominal rotation center of the bipod flexure.

We made an aluminium dummy mirror to test the mechanical performance of the bipod flexure as shown in Fig. 10. The dummy mirror has the same interface and outer dimensions as a 1-m primary mirror. However, the dummy mirror has a fully-closed back surface, which is different from the optical mirror. A thin sheet plate closes the open back and is fixed with an epoxy adhesive. The specific stiffness of aluminium is lower than that of Zerodur®,[16] such that the natural frequencies of the dummy mirror will be lower if it is made the same as the optical mirror. Just by closing the entire back and making simple pocket patterns, the aluminium dummy mirror has the same weight and stiffness as the Zerodur® mirror. On the other hand, the dimensions of the flexure

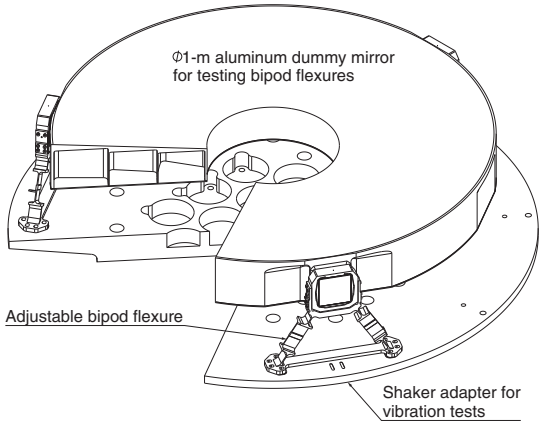

FIG. 10. 1-m dummy mirror mounted on bipod flexures. It is fixed on a shaker adapter for vibration tests.

TABLE I. Comparison of mechanical performances of the bipod flexure for the dummy mirror system.

	Req.	Analytical prediction	FEA	Deviation (%)
Lateral displacement δ (μm)	<20	10.5	11.2	−6.7
Fundamental frequency F1 (Hz)	>120	148.1	142.9	3.5

TABLE II. Modal participation of the dummy mirror system. Fundamental mode at 119.8 Hz has a translation in the x or z direction whose participation is 27.9 % (bold).

Mode	Freq. (Hz)	Tx (%)	Ty (%)	Tz (%)	Rx (%)	Ry (%)	Rz (%)
1	**119.8**	0.07	0.00	**27.9**	8.34	0.00	0.02
2	**119.8**	**27.9**	0.00	0.07	0.02	0.00	8.30
3	211.7	0.00	29.7	0.00	0.00	0.00	0.00
4	213.3	0.00	0.00	0.00	0.00	30.2	0.00
5	233.1	0.00	0.00	0.00	10.4	0.00	10.6
6	233.2	0.00	0.00	0.00	10.6	0.00	10.4
7	492.6	0.01	0.00	0.01	4.19	0.00	6.66
8	492.9	0.01	0.00	0.01	6.64	0.00	4.18
9	581.9	0.00	0.92	0.00	0.00	0.00	0.00
10	586.9	0.00	0.00	0.00	0.03	0.00	0.01
	Total	28.0	30.7	28.0	40.2	30.2	40.0

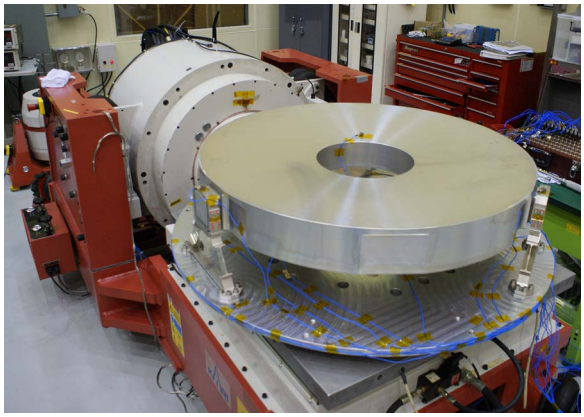

FIG. 11. 1-m dummy mirror system on a shaker for vibration tests.

TABLE III. Comparison of modal frequencies obtained from each axis.

	Prediction (Hz)	Test (Hz)	Deviation (%)	Req. (%)
X-mode	119.8	120	0.2	<5
Y-mode	119.8	118	−1.5	

parameters are optimized to be $t = 1.8$ mm, $l = 50$ mm, $w = 30$ mm, $\psi = 64^\circ$. We compared the mechanical performances from analytical predictions and FEA, which are shown in Table I. Their deviations are less than 10%, and analytical predictions from the proposed equations are proved to be useful even when we add corner fillets to the real flexure design for fabrication.

The dummy mirror is fixed on a shaker adapter for vibration tests. Due to the armature size of a shaker, the adapter has an upside-down trapezoidal shape, which lowers the natural frequency of the test article. We included the shaker adapter for dynamic analysis to predict the natural frequencies considering the fixture effect. The fundamental modes of the dummy mirror system have translations in the x and y directions as their major participations. Modal participation is listed in Table II. Fundamental frequency is the same in both x and z directions, which is the expected result from Eq. (19).

IV. VIBRATION TEST

The vibration test verifies the mechanical safety under launch loads. Computational results using FEA can also be verified by comparing natural frequencies from simulations and experiments. Modal sweep can even detect the adhesive breakage or bolt slips after vibration tests. Figure 11 shows the 1-m dummy mirror system loaded on a shaker for vibration tests. We applied a random vibration profile of which peak load is designed to be 20 g gravity in each axis.

Table III lists the modal frequencies obtained from FEA and vibration tests. Their deviations are less than 1.5%, satisfying the requirement of 5%. The vibration tests were conducted successfully, and there was no change in modal frequencies before and after the tests.

V. CONCLUSIONS

We proposed an analytical formulation of the bipod flexure for mounting the 1-m primary mirror in a space telescope. We described the compliance and stiffness matrices of the bipod flexure and used them for initial flexure design. Parametric exploration of the design space satisfying design requirements was possible without relying on FEA. Experimental verification of the bipod flexure for space application was also achieved by vibration tests with a dummy mirror system. The difference between the analytical results using FEA and the results from vibration test was less than 1.5% in terms of modal frequencies.

APPENDIX: NON-ZERO ELEMENTS OF THE BIPOD'S COMPLIANCE MATRIX

Non-zero elements C_{ij}^{p} of the bipod's compliance matrix in Eq. (11) are presented as below

$$C_{13}^{p} = \frac{18L^2(2t^2+w^2)\mathrm{Cos}\left[\frac{\psi}{2}\right]}{4GJ(2t^2+w^2)+t^3w^3\mathrm{E}+(-4GJ(2t^2+w^2)+t^3w^3E)\mathrm{Cos}[\psi]},$$

$$C_{14}^{p} = \frac{12L(2t^2+w^2)}{4GJ(2t^2+w^2)+t^3w^3E+(-4GJ(2t^2+w^2)+t^3w^3E)\mathrm{Cos}[\psi]},$$

$$C_{25}^{p} = C_{25}^{pn}/C_{25}^{pd},$$

where $C_{25}^{pn} = 6L^3(52t^4+28t^2w^2+w^4)$ and

$$\begin{aligned} C_{25}^{pd} = {} & 104GJL^2t^4+56GJL^2t^2w^2+2GJL^2w^4+6d^2t^2w^2E+40L^2t^5w^3E+3d^2t^3w^5E \\ & +14L^2t^3w^5E+2L^2(GJ(52t^4+28t^2w^2+w^4)-t^3w^3(20t^2+7w^2)E)\cos[\psi] \\ & +18dLt^3w^3(2t^2+w^2)E\sin[\tfrac{\psi}{2}]. \end{aligned}$$

$$C_{31}^{p} = C_{31}^{pn}/C_{31}^{pd},$$

where

$$C_{31}^{pn} = 6L(t^2+2w^2)\mathrm{Cos}\left[\frac{\psi}{2}\right]\left(-9Lt^2w^2+d(-3t^2w^2+L^2(t^2+26w^2))\mathrm{Sin}\left[\frac{\psi}{2}\right]\right) \text{ and}$$

$$C_{31}^{pd} = t^3w^3E\left(6d^2t^2+28L^2t^2+12d^2w^2+80L^2w^2+3t^2w^2+(3t^2w^2-4L^2(7t^2+20w^2))\mathrm{Cos}[\psi]+36dL(t^2+2w^2)\mathrm{Sin}\left[\frac{\psi}{2}\right]\right).$$

$$C_{36}^{p} = C_{36}^{pn}/C_{36}^{pd},$$

where

$$C_{36}^{pn} = -(6L(t^2+2w^2)(-3t^2w^2-L^2(t^2+26w^2)+(-3t^2w^2+L^2(t^2+26w^2))\mathrm{Cos}[\psi]))\text{and}$$

$$C_{36}^{pd} = t^3w^3E\left(6d^2t^2+28L^2t^2+12d^2w^2+80L^2w^2+3t^2w^2+(3t^2w^2-4L^2(7t^2+20w^2))\mathrm{Cos}[\psi]+36dL(t^2+2w^2)\mathrm{Sin}\left[\frac{\psi}{2}\right]\right).$$

$$C_{41}^{p} = C_{41}^{pn}/C_{41}^{pd},$$

where

$$\begin{aligned} C_{41}^{pm} = {} & 3L(d^2L^2t^4+28d^2L^2t^2w^2+3d^2t^4w^2+56L^2t^4w^2+52d^2L^2w^4+6d^2t^2w^4+160L^2t^2w^4 \\ & +d^2(t^2+2w^2)(-3t^2w^2+L^2(t^2+26w^2))\cos[\psi]+36dLt^2w^2(t^2+2w^2)\sin[\tfrac{\psi}{2}]) \text{ and} \end{aligned}$$

$$C_{41}^{pd} = 2t^3w^3\mathrm{E}\left(6d^2t^2+28L^2t^2+12d^2w^2+80L^2w^2+3t^2w^2+(3t^2w^2-4L^2(7t^2+20w^2))\mathrm{Cos}[\psi]+36dL(t^2+2w^2)\mathrm{Sin}\left[\frac{\psi}{2}\right]\right).$$

$$C_{46}^{p} = \frac{6L(t^2+2w^2)\cos[\frac{\psi}{2}](-9Lt^2w^2+d(-3t^2w^2L^2(t^2+26w^2))\sin[\frac{\psi}{2}])}{t^3w^3E(6d^2t^2+28L^2t^2+12d^2w^2+80L^2w^2+3t^2w^2+(3t^2w^2-4L^2(7t^2+20w^2))\cos[\psi]+36dL(t^2+2w^2)\sin[\frac{\psi}{2}])},$$

$$C_{52}^{p} = \frac{3L^3\left(t^2+26w^2\right)}{twE\left(3t^2w^2+L^2\left(t^2+26w^2\right)+\left(-3t^2w^2+L^2\left(t^2+26w^2\right)\right)\mathrm{Cos}\left[\psi\right]\right)},$$

$$C_{63}^{p} = \frac{2L^3(GJ(52t^4+28t^2w^2+w^4)+t^3w^3(20t^2+7w^2)E-(GJ(52t^4+28t^2w^2+w^4)-t^3w^3(20t^2+7w^2)E)\cos[\psi])}{t^3w^3E(4GJ(2t^2+w^2)+t^3w^3E+(-4GJ(2t^2+w^2)+t^3w^3E)\cos[\psi])},$$

$$C_{64}^{p} = \frac{18L^2\left(2t^2+w^2\right)\mathrm{Cos}\left[\frac{\psi}{2}\right]}{4GJ\left(2t^2+w^2\right)+t^3w^3E+\left(-4GJ\left(2t^2+w^2\right)+t^3w^3\mathrm{E}\right)\mathrm{Cos}\left[\psi\right]}.$$

[1]P. R. Yoder, Jr., "Mounting large, horizontal-axis mirrors," in *Opto-Mechanical Systems Design* (SPIE Press, 2006), pp. 481–502.
[2]Y. K. Yong, T.-F. Lu, and D. C. Handley, "Review of circular flexure hinge design equations and derivation of empirical formulations," Precis. Eng. **32**, 63–70 (2008).
[3]Y. Tian, B. Shirinzadeh, D. Zhang, and Y. Zhong, "Three flexure hinges for compliant mechanism designs based on dimensionless graph analysis," Precis. Eng. **34**, 92–100 (2010).
[4]N. Lobontiu, J. S. N. Paine, E. Garcia, and M. Goldfarb, "Corner-filleted flexure hinges," J. Mech. Des. **123**, 346–352 (2001).
[5]L. Furey, T. Dubos, D. Hansen, and J. Samuels-Schwartz, "Hubble space telescope primary-mirror characterization by measurement of the reflective null corrector," Appl. Opt. **32**, 1703–1714 (1993).
[6]T. Pamplona, Ch. Rossin, L. Martin, G. Moreaux, E. Prieto, P. Laurent, E. Grassi, J-L. Boit, L. Castinel, J. Garcia, and B. Milliard, "Three bipods slicer prototype: Tests and finite element calculations," Proc. SPIE **7018**, 701828 (2008).
[7]E. T. Kvamme and M. T. Sullivan, "A small low-stress stable 3-DOF mirror mount with one arc-second tip/tilt resolution," Proc. SPIE **5528**, 264–271 (2004).
[8]H. Kihm, H.-S. Yang, I. K. Moon, J.-H. Yeon, S.-H. Lee, and Y.-W. Lee, "Adjustable bipod flexures for mounting mirrors in a space telescope," Appl. Opt. **51**, 7776–7783 (2012).
[9]Y. Wu and Z. Zhou, "Design calculations for flexure hinges," Rev. Sci. Instrum. **73**, 3101–3106 (2002).
[10]Y. M. Tseytlin, "Notch flexure hinges: An effective theory," Rev. Sci. Instrum. **73**, 3363–3368 (2002).
[11]K.-B. Choi and C. S. Han, "Optimal design of a compliant mechanism with circular notch flexure hinges," Proc. Inst. Mech. Eng., Part C: J. Mech. Eng. Sci. **221**, 385–392 (2007).
[12]W. O. Schotborgh, F. G. M. Kokkeler, H. Tragter, and F. J. A. M. van Houten, "Dimensionless design graphs for flexure elements and a comparison between three flexure elements," Precis. Eng. **29**, 41–47 (2005).
[13]H.-J. Su, H. Shi, and J. Yu, "A symbolic formulation for analytical compliance analysis and synthesis of flexure mechanism," J. Mech. Des. **134**, 051009 (2012).
[14]H. Kihm and H.-S. Yang, "Design optimization of a 1-m lightweight mirror for a space telescope," Opt. Eng. **52**, 091806 (2013).
[15]H. Kihm, H.-S. Yang, and Y.-W. Lee, "Optomechanical analysis of a 1-m light-weight mirror system," J. Korean Phys. Soc. **62**, 1239–1246 (2013).
[16]P. R. Yoder, Jr., *Mounting Optics in Optical Instruments*, 2nd ed. (SPIE Press, 2008).